Effect of surface structure on peptide adsorption on soft surfaces

D. L. Cheung[a]

[a]*School of Chemistry, National University of Ireland Galway, University Road, Galway, Ireland*

Abstract

Understanding protein adsorption onto material surfaces is a major challenge in the design of biomaterials. While this has been long studied knowledge of how the nanoscale surface structure affects protein adsorption is lacking. Using molecular dynamics simulations the effect of nanoscale structure, specifically alternating hydrophobic and hydrophilic stripes, on on the adsorption of LK-peptides onto surfaces is investigated. Strongest adsorption is found for surfaces with larger hydrophobic regions, which allow the peptides to minimise unfavourable contacts with hydrophilic regions. This information may be used to understand the relationship between protein adsorption and surface structure.

1. Introduction

Adsorption of proteins onto material surfaces is the initial event that occurs when a synthetic object comes into contact with a biological system. As this often triggers an immune response that dictates the eventual fate of the system, understanding the interaction between the material surface and proteins is vital for the design of novel materials to be used in medical devices. Much effort has been used in the pursuit of materials that resist the adsorption of proteins[1]. There has been particular interest the development of soft surfaces, such as self-assembled monolayers[2] (SAM) or polymer brushes[3], as their ease of modification allows them to be tailored for specific applications. Considerable synthetic effort has been expended over a number of years and a variety of protein resistant surfaces have been developed. A few guidelines for the design of biocompatible surfaces have been proposed[4] (e.g. charged, hydrophilic materials) but exceptions to these exist[5], so understanding the basis for the design of biocompatible surface coatings is an on going concern.

Changes to the surface structure many also affect the adsorption of proteins. This is common in biological systems, where biointerfaces, such as the cell membrane, often possess nanoscale structure. One synthetic approach involves the

Email address: david.cheung@nuigalway.ie (D. L. Cheung)

use of mixtures of positively and negatively charged molecules, leading to a zwitterionic surface[6]. This leads to strong water structuring and reduces the surface dipole, both factors that are expected to reduce protein adsorption[7]. There has also been interest in the creation of surfaces containing incompatible ligands, such as mixtures of hydrophilic and hydrophobic molecules[8], or hydrocarbon- fluorocarbon mixtures[9]. The differing chemistry of the molecules may give these surfaces characteristics significantly different to uniform ones[10]. However, it can be difficult to control demixing between different types of ligand molecules, so large-scale preparation of well-defined surfaces is difficult. This makes it experimentally difficult to relate protein adsorption to the nanoscale topology. Recently the use of bidentate ligands with both hydrophobic and hydrophilic end groups has allowed for the construction of surfaces with incompatible ligands with controlled nanoscale topology[11, 12, 13], with feature sizes on the molecular length scales. As this is comparable in size to proteins it may be expected that the interaction between these surfaces and biomolecules may be significantly different to uniform surfaces. Indeed properties of such structured surfaces, such as the surface free energy, depend on their structure in a non-trivial manner [14]. Changing the sizes of the surface features may provide an alternative route to control biomolecule-surface interactions.

While a range of experimental methods have been applied to the study of protein adsorption onto surfaces, the limited time and spatial resolution of these means that knowledge of the initial stages of protein adsorption is still lacking. Molecular simulation operates directly on the molecular level and so can give microscopic information regarding the behaviour of proteins at surfaces, such as determining adsorption strengths of proteins[15, 16] and identifying key residues involved in the adsorption process[17]. It has been used to investigate adsorption of proteins onto a range of different surfaces[18, 19], including metals, inorganic materials, and polymer surfaces. A number of studies of protein adsorption onto self-assembled monolayers have been performed[20, 21, 15, 22, 16, 23, 24], demonstrating that adsorption free energies in good agreement with experimental can be obtained. In particular the importance of adequately sampling the protein conformations near the surface has been demonstrated[15, 16]. The changes in protein conformation at interfaces, necessary for understanding the subsequent formation of interfacial layers has also been investigated for small proteins. While previous studies have largely focused on uniform monolayers a few simulations of protein adsorption onto mixed SAMs have been performed, including the investigation of cytochrome-C on mixed monolayer protected nanoparticles [25] and the hydrophobin EAS adsorbed on nanopatterned surfaces [26]. These studies have given insight into the effect of changing surface patterning on protein adsorption, in particular identifying the role played by the amphipathic character of lysine residues. However, as these focused on specific experimental systems they were unable to give insight into the generic effect of surface structure and protein adsorption. Also the sizes of proteins considered meant that these were unable to determine the adsorption free energy, a crucial quantity in understanding the adsorption process, or to examine large-scale changes in protein conformation during adsorption.

In this paper molecular dynamics simulations are used to investigate the adsorption of model peptides onto nanostructured surfaces, specifically consisting of stripes containing hydrophilic and hydrophobic ligands. The peptides are examples of the so-called LK-peptides[27], short sequences consisting of leucine (hydrophobic) and lysine (hydrophilic) residues. Depending on the spacing between the hydrophobic residues these form α-helix or β-strands at hydrophobic interfaces. The surface was composed of a SAM consisting of alkylthiol molecules with differing functional groups on the outside. Alongside uniformly hydrophobic (CH_3-terminated) and hydrophilic (OH-terminated) surfaces, nanostructured surfaces, consisting of stripes of hydrophobic and hydrophilic ligands, were constructed. The stripe widths of approximately 4.3 Å to 21.6 Å (corresponding to between one and five molecules) were investigated. Using metadynamics simulations the adsorption strengths of the model peptides on these surfaces are determined, with the factors that control the adsorption strength investigated.

2. Simulation details

The simulated system consists of a single peptide molecule, in proximity to a self-assembled monolayer of varying functionality. Two different peptides are studied, these being LKβ_{15} (LKLKLKLKLKLKLKL) and LKα_{14} (LKKLLKLLKKLLKL), which are designed sequences that form β-strands (LKβ_{15}) or α-helices (LKα_{14}) at interfaces and surfaces[27]. The surface consists of 280 alkylthiol ($SHC_{11}H_{22}$-R, with R=CH_3 or OH) molecules, arranged in a 20×14 array. Surfaces are either homogeneous, solely containing either hydrophobic (CH_3) or hydrophilic (OH) end groups, or striped, with widths of 5, 2, and 1 molecules. The different surfaces are denoted SAMch3, SAMoh, SAM5, SAM2, and SAM1, respectively. The chains were arranged in the $\sqrt{3} \times \sqrt{3}$ R3 geometry, using structures provided by the Latour research group (`https://cecas.clemson.edu/latourlabs/Jmol/Surfaces.html`), mimicking the structure of alkylthiol molecules on a Au111 surface. The same arrangement of chains was used for all surfaces (irrespective of the terminal functional groups). While the spacing between the different ligands in experimental systems may differ from using a consistent arrangement means that changes in peptide behaviour are due to the surface patterning, rather than from changes to the packing of surface ligands. The similarity in size between the methyl and hydroxy groups is also likely to render changes in the ligand packing small. The positions of the terminal sulfur and hydrogen atoms in the SAMS are fixed, mimicking strong adsorption onto an underlying substrate. For all surfaces an energy minimization and short MD simulation was performed prior to the introduction of the peptides. The peptide and SAM are solvated with approximately 9400 water molecules, with Cl^- counter-ions added to neutralise the system. The system was periodic in the x and y directions while in the z-direction repulsive walls were used to confine the system. To model the system the Charmm36[28, 29, 30, 31] force field is used, with the charmm-variant of the TIP3P water model[32] used for the water. The charmm general force field[33] was used for the alkylthiol molecules.

The simulations were performed in the NVT-ensemble with the temperature controlled using a velocity rescaling algorithm [34] (relaxation time 0.1 ps) at T=300 K. The simulation timestep was 2 fs. Bond lengths were constrained using the LINCS algorithm [35]. All systems were energy minimized using the steepest descent algorithm, followed by a short NVT simulation (20 ps) with the heavy atoms in the proteins restrained to their initial positions using harmonic potentials with a force constant of 2.4 kcal mol^{-1} Å^{-2}. Following this a short NVT simulation (20 ps), without restraining the heavy atoms, was performed.

For the calculation of the adsorption free energy well-tempered metadynamics[36] (MTD) combined with replica exchange with solute tempering[37] (REST) was used. The use of metadynamics allows for the calculation of the free energy surface, with REST being used to enhance sampling of different peptide conformations. In the well-tempered metadynamics simulations two collective variables were used for each set of simulations[16]. The first was the peptide centre-of-mass-surface separation. The surface was defined as the average z position of the terminal heavy atom (either carbon or oxygen) in the alkylthiol chains.

The second collective variable was used to bias the peptide structure. For LKα_{14} this CV is the number of α-helical hydrogen bonds ($N_{\alpha-HB}$), calculated from

$$N_{\alpha-HB} = \sum_{i=1}^{N_{HB}} \frac{1-(r_i/r_0)^n}{1-(r_i/r_0)^m} \tag{1}$$

where the sum runs over the α-helical hydrogen bonds, $n = 8$, $m = 12$, and $r_0 = 2.5$ Å. The switching function in Equation 1 goes from 1 as $r \to 0$ and 0 as $r \to \infty$ and is a continuous approximation to the Heaviside function.

For LKβ_{15} the second CV is the dihedral offset given by

$$DH = \frac{1}{2} \sum_{i=1}^{N-1} \left(1 + \cos\left(\phi_i - \phi_{ref}\right) + \left(1 + \cos(\psi_i - \psi_{ref})\right)\right. \tag{2}$$

where the sum runs over the residues in the peptide and ϕ_i and ψ_i are the ϕ and ψ angles of the ith residue. The reference angles have values $\phi_{ref} = -2.36$ rad and $\psi_{ref} = 2.36$ rad, which correspond to an ideal β-strand with the leucine and lysine side chains being on opposite sides of the peptide backbone.

REST is a variation on replica exchange molecular dynamics[38] where the temperature of only a subset of the system, in this case the protein, varies between replicas. This allows for the use of a smaller number of replicas compared to standard REMD. The temperature scaling is accomplished by scaling the peptide-peptide and peptide-system interactions; the potential energy is given by

$$E_i = \beta_i E_{pp} + \beta_i^{1/2} E_{ps} + E_{ss} \tag{3}$$

where E_{pp} is the peptide-peptide interaction, E_{ps} is the interaction between the peptide and the remainder of the system (water and SAM), and E_{ss} the interaction within the rest of the system. The scaling factor is given by $\beta_i = T_0/T_i$. In these simulations 12 replicas were used, with scaling factors β_i 1.0 (300

K), 0.955 (314 K), 0.911 (329 K), 0.870 (345 K), 0.830 (361 K), 0.793 (378 K), 0.757 (396 K), 0.722 (415 K), 0.690 (435 K), 0.658 (456 K), 0.629 (477 K), and 0.6 (500 K). The metadynamics weight function evolved independently in each replica. A similar combination of REST with well tempered metadynamics was used to determine the adsorption free energy of small peptides onto inorganic surfaces[39, 40] surfaces.

Exchanges between replicas were attempted every 500 timesteps (1 ps). The bias function was updated every 500 timesteps and a bias factor $\gamma = (T + \Delta T)/T = 20$ was used. Following previous work[16] the Gaussian height was 0.956 kcal mol^{-1} and the widths were σ_z=0.1 Å, $\sigma_{alpha-HB} = 0.4$, and $\sigma_{DH} = 0.1$.

All simulations were performed using the Gromacs MD package (v4.6.7)[41]. A modified version of the PLUMED library[42, 43] was used to implement the metadynamics and REST algorithms following Ref. [43]. Standard gromacs tools were used to create the simulation input files. Analysis was performed using standard gromacs tools, VMD[44], and with inhouse scripts using the MDAnalysis package[45].

Simulations were run for 200 ns; convergence of the bias potential was determined by monitoring the RMSD in the bias potential taken at intervals of 10 ns. For all simulations this was consistently below 0.01 kcal mol^{-1} at 200 ns. Following this 100 ns simulations with a constant bias potential were performed for each system, which were used to determine average properties (following removal of the bias potential). Specifically the average value of a property X is calculated using[46]

$$\langle X \rangle = \frac{\sum_i X_i \exp\left[-\beta F\left(\{CV_i\}\right)\right]}{\sum_i \exp\left[-\beta F\left(\{CV_i\}\right)\right]} \tag{4}$$

where X_i is the value at ith data set, F is the free energy, $\{CV_i\}$ are the collective variables used to describe the peptide conformation, and $\beta = 1/k_{\mathrm{B}}T$. Uncertainties in these quantities were estimated using the standard deviation $\sigma_X = \sqrt{\langle X^2 \rangle - \langle X \rangle^2}$. Note that all analysis was performed on neutral ($\beta_i = 1$) replica, as due to the scaling of interactions involving the peptides this is the only one that corresponds to the physical system.

3. Results

3.1. Peptide-surface Interaction

Shown in Figure 1(a) are the free energy profiles for LKβ_{15} and LKα_{14}. For both peptides strong adsorption is seen for the hydrophobic surface, consistent with previous simulation studies. While LKβ_{15} shows only a single minimum near the surface, LKα_{14} has a number of closely spaced minima, which may arise due to different peptide conformations near the surface. Adsorption is significantly weaker for the OH-terminated SAM; for LKβ_{15} there is a shallow minimum (~ -15 kcal mol^{-1}) approximately 4 Å from the surface. The interaction between LKα_{14} and the SAMoh surface is largely repulsive. The values of adsorption free energy are similar to those determined in previous work[15, 16].

For the structured surfaces the free energy profile shows a strong dependence on the stripe width. The thickest stripes (SAM5) have free energy profiles similar to the uniformly hydrophobic surface. In this case it may be expected that the stripe is thick enough for the peptides to largely interact with the hydrophobic regions on the surface, minimising its exposure to the hydrophilic hydoxyl groups. As the stripes get thinner the depth of the free energy minimum decreases, getting closer to the uniformly hydrophilic surface.

The net adsorption free energy ($\Delta_{ads}F$) was calculated using[21, 47]

$$\Delta_{ads}F = -RT \ln \left(\frac{c_{ads}}{c_{bulk}} \right) \tag{5}$$

where the adsorbed and bulk concentrations are given by

$$c_{ads} = \frac{1}{z_0 - z_{min}} \int_{z_{min}}^{z_0} dz \ \exp\left[-\beta F(z)\right] \tag{6a}$$

$$c_{bulk} = \frac{1}{z_{max} - z_0} \int_{z_0}^{z_{max}} dz \ \exp\left[-\beta F(z)\right] \tag{6b}$$

where z_0=10 Å. For both peptides $\Delta_{ads}F$ is lowest for the hydrophobic methyl-terminated SAM, with the value of SAM5 similar (Figure 1(b)). As the stripe thickness decreases $\Delta_{ads}F$ increases, indicating again that the adsorption strength of the peptides decrease as the surface structure goes to smaller sizes. This is consistent with experimental investigation of fibrinogen adsorption onto structured surfaces formed by bidentate ligands with hydrophilic and hydrophobic end groups [12]. For the thinnest stripes $\Delta_{ads}F$ is similar to that for the hydrophilic hydroxyl-terminated SAM.

3.2. Peptide conformation

The free energy protiles (Figure 1) suggest that both peptides exhibit multiple conformations at the surface. The conformation of the peptides at the surface can be investigated through the orientations of the amino acid side chains (defined as the angle θ between the unit vector joining the Cα atom and the Cδ (LEU) or Nζ (LYS) atoms and the z-axis). Shown in Figure 2 are the average $\cos\theta$ for each residue. The uniform surfaces (SAMch3 and SAMoh) behave consistently with previous experimental[48] and computational[16] studies. For the SAMch3 surface the LEU sidechains typically point towards the surface (Figure 2) due to the hydrophobic interaction between these. For LKβ_{15} this is reasonably uniform across the length of the peptide, while the LEU residue at the N-terminus of LKα_{14}, which precedes two hydrophilic LYS residue, shows a reduced tendency to point towards the surface. The sidechain orientation for the SAMoh surface is less well-defined as the LYS sidechains which would be preferentially attracted to this surface are also well solvated in water. Rather, for both peptides, adsorption is mediated by leucine residues (L7 and L11 for LKβ_{15} and L5 and L12 for LKα_{14}). For the thickest stripes (SAM5) the sidechain orientations are similar to the SAMch3 surface, with the LEU residues typically oriented towards the surface.

Similarly the introduction of surface structure leads to changes in the peptide secondary structure. Shown in Figure 3 are the secondary structure propensities (calculated using the STRIDE algorithm) for the different surfaces. For LKβ_{15} stripy surface induces the formation of helical structures. Conversely the stripy surface typically disrupts α-helix formation for LKα_{14}. Compared to bulk solution the surfaces, in particular those with larger hydrophobic regions, typically induce more ordered secondary structure.

Changing surface structure may also change the overall size of the peptides. Shown in Table 1 are the radii of gyration for the peptides on different surfaces. This was calculated only for cases where the peptide was in contact with the surface, using the criteria that the peptide-surface separation was less than 10 Å (alternative definitions, such as ensuring at least one contact between a peptide and surface atom exists, give similar results). For LKβ_{15} R_g is approximately the same for both uniform surfaces, while LKα_{14} is larger on SAMoh than SAMch3 surfaces, suggesting a distortion of the helical structure formed on the hydrophobic surface. Introducing surface structure leads both peptides to adopt more compact structures.

	R_g / Å	
Surface	LKβ_{15}	LKα_{14}
SAMch3	10±1.2	10±1.3
SAMoh	10±2	12±1
SAM5	8.6±0.6	8.0±0.6
SAM2	9±1	8.8±0.4
SAM1	9.4±0.9	9.4±0.9

Table 1: Radius of gyration for surface bound conformations.

Visualisation of the most probable conformations (Figure 4), found using a cluster analysis on surface bound conformations (using the method of Daura[49] with a cut off of 3 Å), shows that the peptides preferentially adopt structures that maximise contact between hydrophobic residues and the methyl terminated chains. For SAMch3 this leads to the peptides adopting conformations that are flat on the surface, which for LKα_{14} leads to distortions from a completely α-helical structure. Similar behaviour is also seen for the SAM5 surface. For the other surfaces the peptides adopt conformations that typically have only a few residues are in contact with the surface. Only for LKβ_{15} on the SAM2 surface does the peptide lie flat on the surface.

Considering the different types of peptide-surface contacts shows that leucine residues are more likely be in contact with the surface (contacts defined using the weight function in Equation 1 with $r_0 = 4.5$ Å). Due to its amphiphilic side chain lysine contacts with both surface ligands[26]. For both peptides the number of contacts with the surface is lower for the hydrophilic surface than hydrophobic surface. As the stripes on the surface decrease in width there is also a decrease in the number of contacts, with the number of hydrophobic con-

Peptide	Surface	N_{total}	$N_{CH3-LEU}$	$N_{CH3-LYS}$	N_{OH-LYS}
	SAMch3	59±11	50±6	9±5	0
	SAMoh	9±5	0	0	9±5
LKβ_{15}	SAM5	39±7	34±5	3±1	2±1
	SAM2	35±9	24±4	5±2	6±3
	SAM1	26±6	18±4	4±1	4±1
	SAMch3	53±8	48±6	5±2	0
	SAMoh	10±4	0	0	10±4
LKα_{14}	SAM5	41±8	36±6	3±1	2±1
	SAM2	34.7±0.7	28±4	2.7±0.7	4±2
	SAM1	26±6	18±4	4±1	4±1

Table 2: Numbers of peptide-surface contacts.

tacts decreasing without a corresponding increase in the number of hydrophilic contacts (Table 2).

3.3. Water structure on mixed SAMS

A large contribution to the anti-fouling behaviour of surfaces is thought to arise due to the presence of a dense water layer near the surface[4, 50]. The density profile of water is shown in Figure 5(a). For the uniform surfaces there is a peak in $\rho_{water}(z)$ near the SAM surface. The height of this peak is slightly higher for hydroxyl-terminated SAM, with this peak also occurring closer to the SAM surface. The structured surfaces show two peaks near the surface, corresponding to the water molecules close to the terminal hydroxyl and methyl groups. For all stripe widths the peak corresponding to the methyl-terminated molecules has approximately the same height and location. The peak corresponding to water molecules near hydroxyl groups gets larger but moves further away from the surface, gradually merging with the other peak.

The amount of water adsorbed on the surface can be quantified through the adsorbance (Γ)

$$\Gamma = \frac{1}{z_2 - z_1} \int_{z_1}^{z_2} dz \ (\rho(z) - \rho_b) \tag{7}$$

where $\rho(z)$ is the water density profile and ρ_b is the bulk density of water. The integral runs from the peak in the density profile for the terminal heavy atoms in the SAM ($z_1 \approx 16.8$ Å) to $z_2 = 40$ Å. As may be expected the adsorbance is highest for the hydrophilic hydroxyl-terminated SAM and lowest for the methyl-terminated SAM. For the mixed surfaces Γ lies between these and is approximately the same for the different stripe widths. This suggests that the amount of water molecules near the surface plays only a minor role in determining the adsorption free energy for the structured surfaces.

The change in the water density profile and adsorbance examine the water structure averaged over the surface it is also useful to investigate how the structure around the hydrophobic and hydrophilic parts of the surface changes with

the stripe thickness. As the stripe width decreases the peak on the C13-water RDF (Figure 5(c)) increases due to water molecules that are close to hydroxyl groups in the OH-terminated molecules. The O13-water RDF shows less variation with the stripe width (Figure 5(d)), due to the strong interaction between water molecules and the OH groups.

4. Conclusions

Using molecular dynamics simulations, employing advanced sampling methods, I investigated the interaction between peptides and nanostructured surfaces. The adsorption strengths were found to depend both on the chemistry of the surface (changing from hydrophobic to hydrophilic) and the surface structure. Strongest adsorption is found for surfaces with larger hydrophobic regions as this allows for the hydrophobic interactions with the LEU side chains. As the stripe widths get smaller the adsorption strength decreases, with it becoming similar to that for a uniformly hydrophilic surface for the thinnest stripes. Qualitative, as well as quantitative, differences were found between the two peptides studied, showing that the interplay between peptide and surface structures affects the adsorption behaviour.

Adsorption of peptides onto the surface leads to changes in their conformation. For surfaces with larger hydrophobic regions (SAMch3 and SAM5) the peptide conformation can be rationalized through the hydrophobic leucine side chains pointing towards the hydrophobic surface. This conformation becomes disrupted as the stripes get narrower. Only small changes are seen in the water structure for the different mixed SAMs so this is less likely to play a role (although it may be important in determining the differing adsorption strengths between the hydrophobic and hydrophilic surfaces).

Both components of the systems studied in this work, the peptides and surfaces, represent idealised model systems. In particular, differences in packing between different ligands and mobility of ligands on the surface would need to be considered to investigate experimental systems. Additionally, the prescence of salts Nonetheless it has revealed details of the relationship between nanoscale surface structure and protein adsorption strength. In future work this will be extended to consider more realistic models of the surface, along with different realisations of surface heterogeneity. Likewise it would be useful to consider more complex proteins, to give more information on the interplay between protein and surface structure. This would give insight into the use of nanostructured surfaces in prevention of protein adsorption in biomaterials and antifouling applications, as well as linking surface structure to the functionality of adsorbed proteins and formation of supramolecular protein structures at surfaces.

Acknowledgements

I wish to acknowledge the Latour research group (Clemson University) for providing downloadable SAM structures. This work was performed on computational facilities provided by the SFI/HEA Irish Centre for High-End Computing

(ICHEC). Modified version of the PLUMED library was provided by Giovanni Bussi (`https://github.com/GiovanniBussi/plumed2`).

Appendix - Demultiplexed simulations

To test the exploration of different conformations in the static bias simulations the variation in the collective variables across the static bias simulations is investigated (Figures 6 and 7). These were performed on the demultiplexed trajectories (using the gromacs demux script). All systems contain trajectories that sample a wide range of CV values, suggesting that the sufficient sampling of protein-surface separations and protein conformation occurred during the simulations.

References

[1] C. Blaszykowski, S. Sheikh, M. Thompson, Surface chemistry to minimize fouling from blood-based fluids, Chemical Society Reviews 41 (17) (2012) 5599.

[2] M. Mrksich, G. M. Whitesides, Using Self-Assembled Monolayers to Understand the Interactions of Man-made Surfaces with Proteins and Cells, Annual review of biophysics and biomolecular structure 25 (2003) 55–78.

[3] N. Ayres, Polymer brushes: Applications in biomaterials and nanotechnology, Polym. Chem. 1 (6) (2010) 769–777.

[4] S. Chen, L. Li, C. Zhao, J. Zheng, Surface hydration: Principles and applications toward low-fouling/nonfouling biomaterials, Polymer 51 (23) (2010) 5283–5293.

[5] C. Rodriguez-Emmenegger, E. Brynda, T. Riedel, M. Houska, V. Šubr, A. B. Alles, E. Hasan, J. E. Gautrot, W. T. S. Huck, Polymer Brushes Showing Non-Fouling in Blood Plasma Challenge the Currently Accepted Design of Protein Resistant Surfaces, Macromolecular Rapid Communications 32 (13) (2011) 952–957.

[6] R. E. Holmlin, X. Chen, R. G. Chapman, S. Takayama, G. M. Whitesides, Zwitterionic SAMs that Resist Nonspecific Adsorption of Protein from Aqueous Buffer, Langmuir 17 (9) (2001) 2841–2850.

[7] S. Chen, F. Yu, Q. Yu, Y. He, S. Jiang, Strong resistance of a thin crystalline layer of balanced charged groups to protein adsorption, Langmuir 22 (19) (2006) 8186–8191.

[8] A. R. Puente Santiago, T. Pineda, M. Blázquez, R. Madueño, Formation of 2-D Crystalline Intermixed Domains at the Molecular Level in Binary Self-Assembled Monolayers from a Lyotropic Mixture, Journal of Physical Chemistry C 120 (16) (2016) 8595–8606.

[9] K.-i. Iimura, T. Shiraku, T. Kato, Micro-Phase Separation in Binary Mixed Langmuir Monolayers of n -Alkyl Fatty Acids and a Perfluoropolyether Derivative, Langmuir 18 (26) (2002) 10183–10190.

[10] A. R. Puente Santiago, G. Sánchez-Obrero, T. Pineda, M. Blázquez, R. Madueño, Influence of Patterning in the Acid-Base Interfacial Properties of Homogeneously Mixed CH3- and COOH-Terminated Self-Assembled Monolayers, Journal of Physical Chemistry C 122 (5) (2018) 2854–2865.

[11] H. J. Lee, A. C. Jamison, T. R. Lee, Two Are Better than One: Bidentate Adsorbates Offer Precise Control of Interfacial Composition and Properties, Chemistry of Materials 28 (15) (2016) 5356–5364.

[12] P. Chinwangso, H. J. Lee, A. C. Jamison, M. D. Marquez, C. S. Park, T. R. Lee, Structure, Wettability, and Thermal Stability of Organic Thin-Films on Gold Generated from the Molecular Self-Assembly of Unsymmetrical Oligo(ethylene glycol) Spiroalkanedithiols, Langmuir 33 (8) (2017) 1751–1762.

[13] M. D. Marquez, O. Zenasni, A. C. Jamison, T. R. Lee, Homogeneously Mixed Monolayers: Emergence of Compositionally Conflicted Interfaces, Langmuir 33 (36) (2017) 8839–8855.

[14] J. J. Kuna, K. Voïtchovsky, C. Singh, H. Jiang, S. Mwenifumbo, P. K. Ghorai, M. M. Stevens, S. C. Glotzer, F. Stellacci, The effect of nanometre-scale structure on interfacial energy., Nature materials 8 (10) (2009) 837–842.

[15] G. Collier, N. A. Vellore, J. A. Yancey, S. J. Stuart, R. A. Latour, Comparison between empirical protein force fields for the simulation of the adsorption behavior of structured LK peptides on functionalized surfaces., Biointerphases 7 (1-4) (2012) 24.

[16] M. Deighan, J. Pfaendtner, Exhaustively Sampling Peptide Adsorption with Metadynamics., Langmuir : the ACS journal of surfaces and colloids 29 (25) (2013) 7999–8009.

[17] D. Mallinson, D. L. Cheung, D. Simionesie, A. B. Mullen, Z. J. Zhang, D. A. Lamprou, Experimental and computational examination of anastellin (FnIII1c)-polymer interactions, Journal of Biomedical Materials Research - Part A 105 (3) (2017) 737–745.

[18] M. Ozboyaci, D. B. Kokh, S. Corni, R. C. Wade, Modeling and simulation of protein-surface interactions: Achievements and challenges, Quarterly Reviews of Biophysics 49 (2016) 1–45.

[19] T. R. Walsh, Pathways to Structure-Property Relationships of Peptide-Materials Interfaces: Challenges in Predicting Molecular Structures, Accounts of Chemical Research 50 (7) (2017) 1617–1624.

[20] J. Zheng, L. Li, S. Chen, S. Jiang, Molecular simulation study of water interactions with oligo (ethylene glycol)-terminated alkanethiol self-assembled monolayers, Langmuir 20 (20) (2004) 8931–8938.

[21] C. P. O' Brien, S. J. Stuart, D. A. Bruce, R. A. Latour, Modeling of Peptide Adsorption Interactions with a Poly (lactic acid) Surface Modeling of Peptide Adsorption Interactions with a Poly (lactic acid), Langmuir 24 (9) (2008) 14115–14124.

[22] Y. Xie, M. Liu, J. Zhou, Molecular dynamics simulations of peptide adsorption on self-assembled monolayers, Applied Surface Science 258 (20) (2012) 8153–8159.

[23] Z. A. Levine, S. A. Fischer, J. E. Shea, J. Pfaendtner, Trp-Cage Folding on Organic Surfaces, Journal of Physical Chemistry B 119 (33) (2015) 10417–10425.

[24] J. Liu, J. Zhou, Hydrolysis-controlled protein adsorption and antifouling behaviors of mixed charged self-assembled monolayer: A molecular simulation study, Acta Biomaterialia 40 (2016) 23–30.

[25] A. Hung, S. Mwenifumbo, M. Mager, J. J. Kuna, F. Stellacci, I. Yarovsky, M. M. Stevens, Ordering surfaces on the nanoscale: Implications for protein adsorption, Journal of the American Chemical Society 133 (5) (2011) 1438–1450.

[26] M. Penna, K. Ley, S. Maclaughlin, I. Yarovsky, Surface heterogeneity: a friend or foe of protein adsorption ? insights from theoretical simulations, Faraday Discuss. 191 (2016) 435–464.

[27] W. DeGrado, J. Lear, Induction of peptide conformation at apolar water interfaces. 1. A study with model peptides of defined hydrophobic periodicity, Journal of the American Chemical Society 107 (10) (1985) 7684–7689.

[28] A. D. MacKerell, D. Bashford, R. L. Dunbrack, J. D. Evanseck, M. J. Field, S. Fischer, J. Gao, H. Guo, S. Ha, D. Joseph-McCarthy, L. Kuchnir, K. Kuczera, F. T. K. Lau, C. Mattos, S. Michnick, T. Ngo, D. T. Nguyen, B. Prodhom, W. E. Reiher, B. Roux, M. Schlenkrich, J. C. Smith, R. Stote, J. Straub, M. Watanabe, J. Wiórkiewicz-Kuczera, D. Yin, M. Karplus, All-Atom Empirical Potential for Molecular Modeling and Dynamics Studies of Proteins †, The Journal of Physical Chemistry B 102 (18) (1998) 3586–3616.

[29] A. D. Mackerell, M. Feig, C. L. Brooks, Extending the treatment of backbone energetics in protein force fields: Limitations of gas-phase quantum mechanics in reproducing protein conformational distributions in molecular dynamics simulation, Journal of Computational Chemistry 25 (11) (2004) 1400–1415.

[30] P. Bjelkmar, P. Larsson, M. A. Cuendet, B. Hess, E. Lindahl, Implementation of the {CHARMM} Force Field in {GROMACS}: Analysis of Protein Stability Effects from Correction Maps, Virtual Interaction Sites, and Water Models, J. Chem. Theory Comput. 6 (2) (2010) 459–466.

[31] R. B. Best, X. Zhu, J. Shim, P. E. M. Lopes, J. Mittal, M. Feig, A. D. MacKerell Jr, Optimization of the Additive CHARMM All-atom Protein Force Field Targeting Improved Sampling of the Backbone ϕ, ψ and Side-chain $\chi 1$ and $\chi 2$ Dihedral Angles, Journal of Chemical Theory and Computation 8 (9) (2012) 3257–3273.

[32] P. Mark, L. Nilsson, Structure and dynamics of the TIP3P, SPC, and SPC/E water models at 298 K, Journal of Physical Chemistry A 105 (43) (2001) 9954–9960.

[33] K. Vanommeslaeghe, E. Hatcher, C. Acharya, S. Kundu, S. Zhong, J. Shim, E. Darian, O. Guvench, P. Lopes, I. Vorobyov, A. D. Mackerell, CHARMM general force field: A force field for drug-like molecules compatible with the CHARMM all-atom additive biological force fields, J. Comput. Chem. 31 (2009) 671–690. doi:10.1002/jcc.21367.
URL `http://doi.wiley.com/10.1002/jcc.21367`

[34] G. Bussi, D. Donadio, M. Parrinello, Canonical sampling through velocity rescaling, Journal of Chemical Physics 126 (1) (2007) 014101/1–7.

[35] B. Hess, H. Bekker, H. J. C. Berendsen, J. G. E. M. Fraaije, LINCS: A linear constraint solver for molecular simulations, Journal of computational chemistry 18 (12) (1997) 1463–1472.

[36] A. Barducci, G. Bussi, M. Parrinello, Well-Tempered Metadynamics: A Smoothly Converging and Tunable Free-Energy Method, Physical Review Letters 100 (2) (2008) 020603–.

[37] P. Liu, B. Kim, R. A. Friesner, B. J. Berne, Replica exchange with solute tempering: a method for sampling biological systems in explicit water., Proceedings of the National Academy of Sciences of the United States of America 102 (39) (2005) 13749–54.

[38] Y. Sugita, Y. Okamoto, Replica exchange molecular dynamics method for protein folding simulation., Chemical Physics Letters 314 (1) (1999) 141–151.

[39] J. Schneider, L. Colombi Ciacchi, Specific material recognition by small peptides mediated by the interfacial solvent structure, Journal of the American Chemical Society 134 (4) (2012) 2407–2413.

[40] L. B. Wright, J. P. Palafox-Hernandez, P. M. Rodger, S. Corni, T. R. Walsh, Facet selectivity in gold binding peptides: exploiting interfacial water structure, Chem. Sci. 6 (9) (2015) 5204–5214.

[41] B. Hess, C. Kutzner, D. van der Spoel, E. Lindahl, GROMACS 4: Algorithms for Highly Efficient, Load-Balanced, and Scalable Molecular Simulation, J. Chem. Theory Comput. 4 (3) (2008) 435–447.

[42] G. A. Tribello, M. Bonomi, D. Branduardi, C. Camilloni, G. Bussi, PLUMED 2: New feathers for an old bird, Computer Physics Communications 185 (2) (2014) 604–613.

[43] G. Bussi, Hamiltonian replica exchange in GROMACS: a flexible implementation, Molecular Physics 112 (3-4) (2013) 379–384.

[44] W. Humphrey, A. Dalke, K. Schulten, VMD: Visual molecular dynamics, Journal of Molecular Graphics 14 (1) (1996) 33–38.

[45] N. Michaud-Agrawal, E. J. Denning, T. B. Woolf, O. Beckstein, MDAnalysis: A Toolkit for the Analysis of MolecularDynamics Simulations, Journal of computational chemistry 32 (10) (2011) 2319–2327.

[46] G. Torrie, J. Valleau, Nonphysical sampling distributions in Monte Carlo free-energy estimation: Umbrella sampling, J. Comput. Phys. 23 (2) (1977) 187–199. doi:10.1016/0021-9991(77)90121-8.

[47] Z. E. Hughes, T. R. Walsh, Distinct Differences in Peptide Adsorption on Palladium and Gold: Introducing a Polarizable Model for Pd(111), J. Phys. Chem. C 122 (34) (2018) 19625–19638.

[48] T. Weidner, D. G. Castner, SFG analysis of surface bound proteins: a route towards structure determination., Physical chemistry chemical physics : PCCP 15 (30) (2013) 12516–24.

[49] X. Daura, K. Gademann, B. Jaun, D. Seebach, W. F. Van Gunsteren, A. E. Mark, Peptide Folding: When Simulation Meets Experiment, Angew. Chemie Int. Ed. 38 (1999) 236–240.

[50] S. Sheikh, C. Blaszykowski, R. Nolan, D. Thompson, M. Thompson, On the hydration of subnanometric antifouling organosilane adlayers: A molecular dynamics simulation, Journal of Colloid and Interface Science 437 (2015) 197–204.

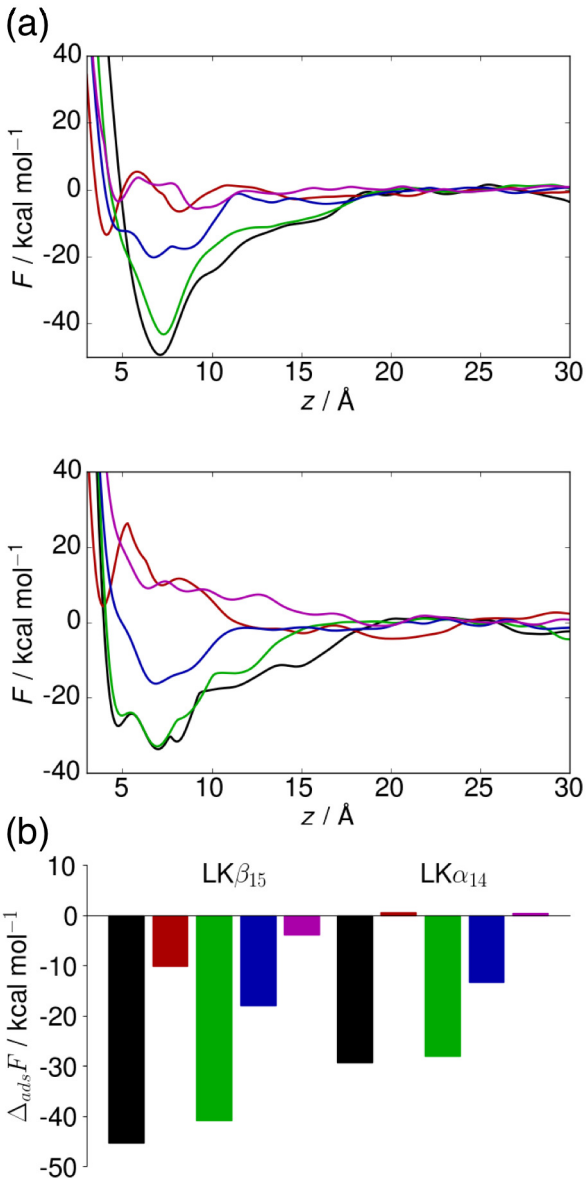

Figure 1: (Colour online) (a) Free energy profiles for LKβ_{15} (top) and LKα_{14} (bottom) (b) net adsorption free energies (bottom). SAMch3, SAMoh, SAM5, SAM2, and SAM1 surfaces denoted by black, red, green, blue, and magenta respectively.

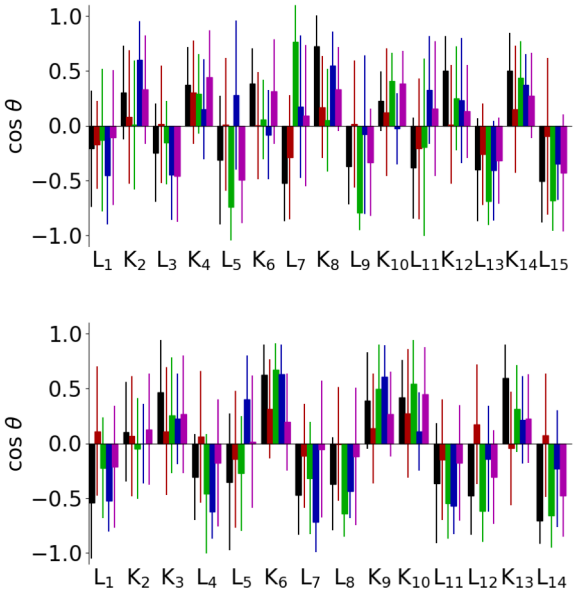

Figure 2: (Colour online) Sidechain orientations for LKβ_{15} (top) and LKα_{14} (bottom) on SAM surfaces. Black, red, green, blue, and magenta denotes SAMch3, SAMoh, SAM5, SAM2, and SAM1 surfaces respectively.

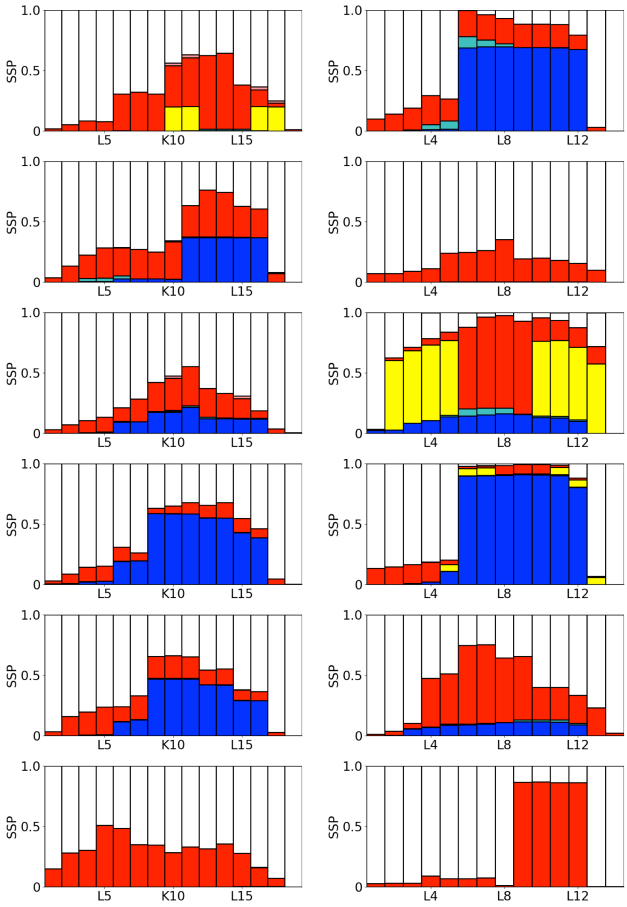

Figure 3: (Colour online) Secondary structure propensities for LKβ_{15} (left) and LKα_{14} (right) on (top to bottom) SAMch3, SAMoh, SAM5, SAM2, SAM1, and bulk solution. α-helix, β-strand, turn, 3/10-helix, and coil denoted by blue, yellow, red, cyan, and white respectively.

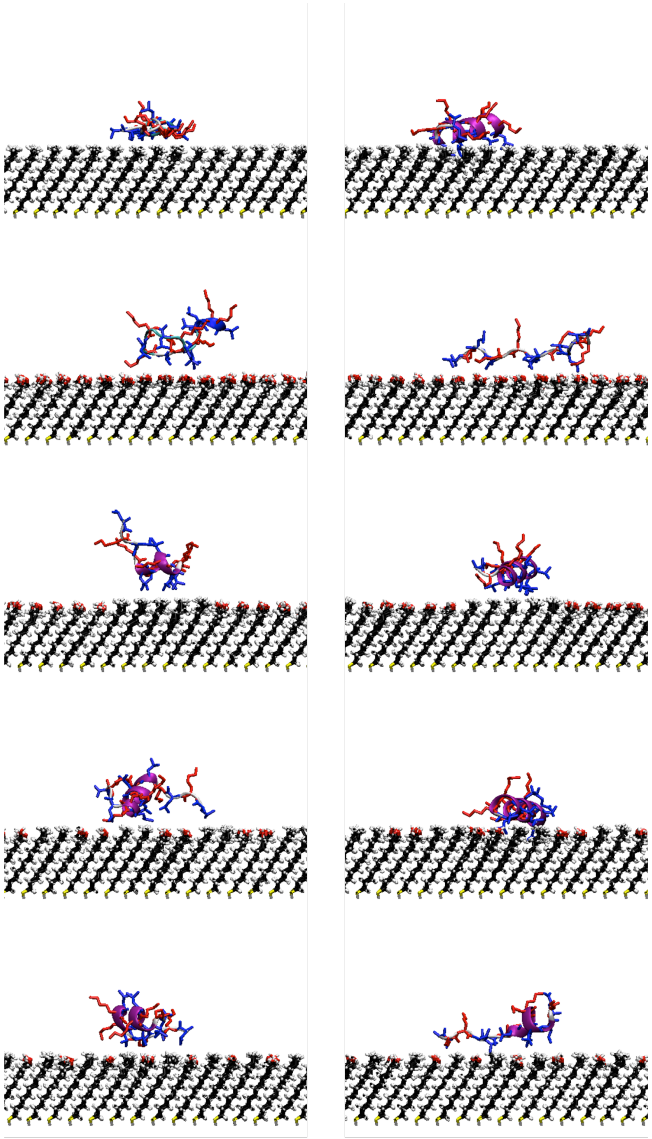

Figure 4: (Colour online) Snapshots showing structures from the most probable clusters for LKβ_{15} (left) and LKα_{14} (right). From top to bottom SAMch3, SAMoh, SAM5, SAM2, and SAM1. Leucine and lysine residues shown in blue and red respectively.

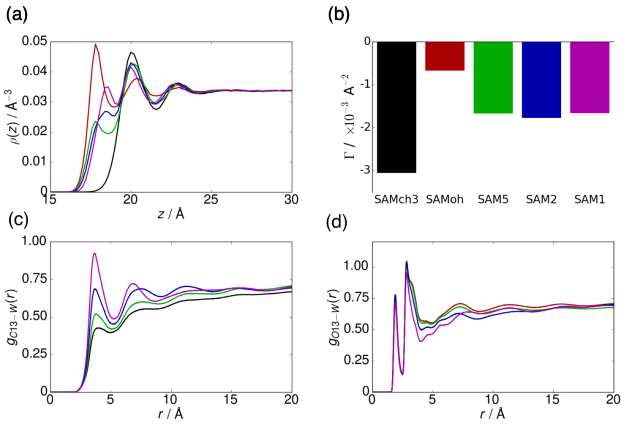

Figure 5: (Colour online) Water structure near self-assembled monolayers. (a) Water density profile (b) Adsorbance (c) Water-C13 radial distribution function (d) Water-O13 radial distribution function. In all cases SAMch3, SAMoh, SAM5, SAM2, and SAM1 are denoted by black, red, green, blue, and magenta respectively.

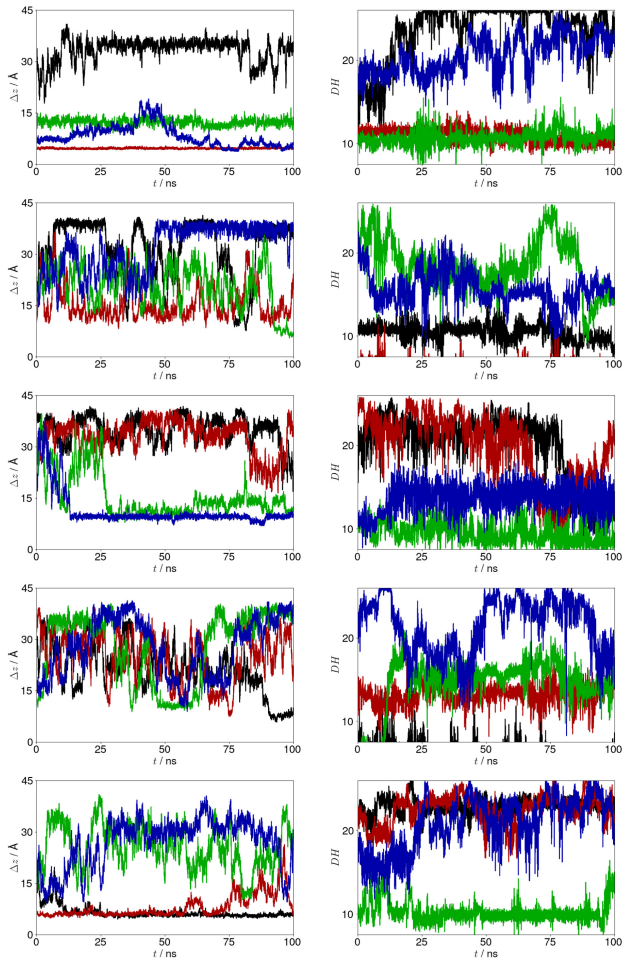

Figure 6: (Colour online) Variation of Δz (left) and DH (right) for demultiplex trajectories of LKβ_{15} from static bias simulations for (top to bottom) SAMch3, SAMoh, SAM5, SAM2, and SAM1. Black, red, green, and blue lines denote the 0th, 3rd, 7th, and 11th replicas.

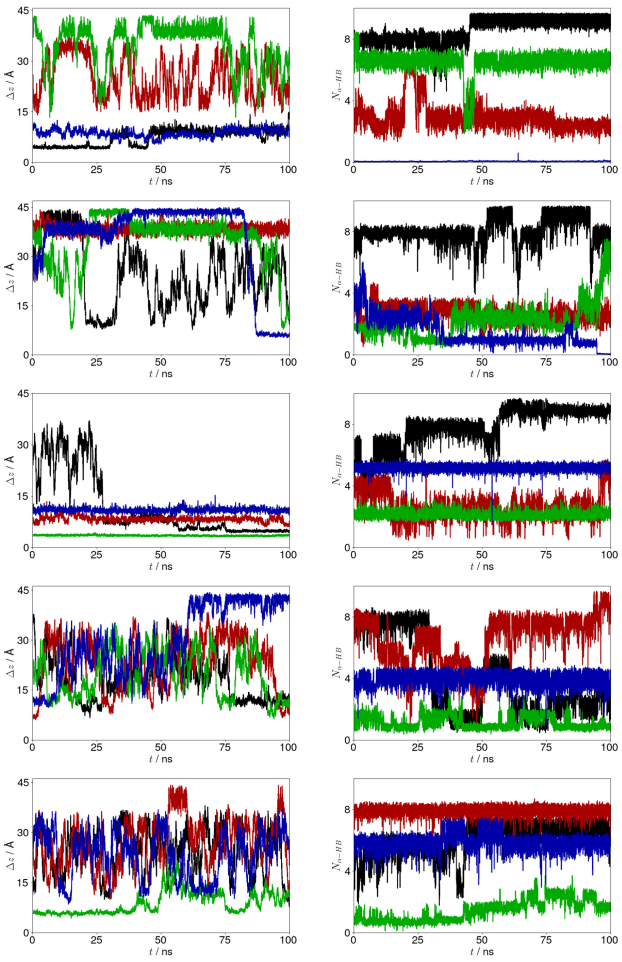

Figure 7: (Colour online) Variation of Δz (left) and $N_{\alpha-HB}$ (right) for demultiplex trajectories of LKα_{14} from static bias simulations for (top to bottom) SAMch3, SAMoh, SAM5, SAM2, and SAM1. Black, red, green, and blue lines denote the 0th, 3rd, 7th, and 11th replicas.